JGR Space Physics

RESEARCH ARTICLE
10.1029/2020JA028861

The Delayed Ionospheric Response to the 27-day Solar Rotation Period Analyzed With GOLD and IGS TEC Data

Erik Schmölter[1], Jens Berdermann[1], and Mihail Codrescu[2]

[1]Institute for Solar-Terrestrial Physics, German Aerospace Center, Neustrelitz, Germany, [2]Space Weather Prediction Center, National Oceanic and Atmospheric Administration, Boulder, CO, USA

Key Points:

- The good correlation of Global-scale Observations of the Limb and Disk (GOLD) extreme ultraviolet (EUV) proxy and GOLD peak electron density with total electron content (TEC) allows detailed studies of the delayed ionospheric response
- The ionospheric delay to the 27-day solar rotation period based on GOLD EUV proxy and TEC confirms recent delay estimates of about 1 day
- GOLD measurements at different times of the day allow insight into ionization, recombination and related accumulation processes

Correspondence to:
E. Schmölter,
Erik.Schmoelter@dlr.de

Citation:
Schmölter, E., Berdermann, J., & Codrescu, M. (2021). The delayed ionospheric response to the 27-day solar rotation period analyzed with GOLD and IGS TEC data. *Journal of Geophysical Research: Space Physics*, *126*, e2020JA028861. https://doi.org/10.1029/2020JA028861

Received 23 OCT 2020
Accepted 8 JAN 2021

Abstract The delayed ionospheric response is analyzed for two well-defined 27-day solar rotation periods in the year 2019 with solar radio flux index F10.7 and Global-scale Observations of the Limb and Disk (GOLD) data, like solar extreme ultraviolet (EUV) flux proxy, O/N_2 column density ratio and peak electron density, as well as International Global Navigation Satellite System Service rapid high-rate total electron content (TEC) map data. Although the correlation between GOLD solar EUV flux proxy and TEC is similar to the correlation between F10.7 and TEC, it is shown that the estimated delays based on GOLD data are in much better agreement with recent studies using EUV measurements compared to the delays based on F10.7 data. The GOLD peak electron density correlates well with TEC and allows insight to a local time interval when the ionosphere is not controlled by solar activity changes (17:00 LT to 21:00 LT). The present study investigates the impact of the solar activity (F10.7, GOLD EUV flux proxy) and O/N_2 column density ratio on the ionospheric delay for two representative solar rotation periods. The capabilities of GOLD data for future research on the ionospheric response to the 27-day solar rotation period are demonstrated and discussed. These results are crucial information for precise ionospheric models and forecasts.

1. Introduction

The absorption of solar extreme ultraviolet (EUV) radiation in the upper atmosphere defines the ionospheric plasma by ionization and heating but also controls the neutral parts of the thermosphere (Kelley, 2009). The photoionization of O, O_2, and N_2, the photodissociation of O_2, and the dissociative photoionization of N_2 are the major processes during the absorption. These processes control the ionospheric state and, thus, the ionospheric response to different variations of the solar activity (Kelley, 2009). The 27-day solar rotation period is a significant variation of the solar activity that is known to impact the ionospheric plasma (Forbes et al., 2000; Kane et al., 1995; Ma et al., 2012; Min et al., 2009; Oinats et al., 2008; Rich, 2003; Rishbeth & Mendillo, 2001). The ionospheric response to these variations is not immediate and a delay of a few hours up to days occurs (Afraimovich et al., 2008; Jakowski et al., 1991, 2002; Lee et al., 2012; Min et al., 2009; Oinats et al., 2008; Ren et al., 2018; Schmölter et al., 2018, 2020; Titheridge, 1973; Zhang & Holt, 2008). Spatial and temporal features of this delayed ionospheric response are of actual scientific interest and are characterized in recent studies (Ren et al., 2018, 2019, 2020; Schmölter et al., 2020) to improve our understanding of physical and chemical processes causing the delay (Ren et al., 2018; Schmölter et al., 2020; Vaishnav et al., 2019).

The delayed ionospheric response to the 27-day solar rotation period of the solar activity is explained by two major absorption processes of the upper atmosphere. The photodissociation of O_2 impacts the density of O and O_2 in the ionospheric F region and can cause the accumulation of O. This accumulation is supposed to result in a change of the ionospheric state causing a delayed response to the change of solar activity (Jakowski et al., 1991, 2002; Titheridge, 1973). The O and N_2 densities and more specifically their ratio define the ion production and loss of the ionospheric plasma (Rishbeth, 1998). While the ion production due to O is almost immediate, the loss due to N_2 is not (Ren et al., 2018). Therefore, solar activity variations cannot cause corresponding changes immediately in the ionospheric plasma at all times (Ren et al., 2018; Schmölter et al., 2020).

Analyzing the delayed ionospheric response based on solar EUV measurements at high temporal resolution (≤1 h) allows to define spatial and temporal variations in detail (Schmölter et al., 2020), but long-term

studies are difficult due to frequent or big data gaps (Schmölter et al., 2018, 2020). Therefore, the combined analysis of several ionospheric and solar parameters is also important to improve the current understanding of the delay.

The recent National Aeronautics and Space Administration (NASA) mission Global-scale Observations of the Limb and Disk (GOLD) provides a set of new data products including a solar EUV flux proxy, the O/N_2 column density ratio and the peak electron density. This combination of measurements is of interest for the analysis of the ionospheric response time to the 27-day solar rotation period. This study presents first results of such an analysis and compares the findings to solar and ionospheric parameters, that have been commonly used in preceding studies. The potential of GOLD data to characterize the delayed ionospheric response is discussed based on these results.

2. Data

This study analyses different solar proxies and ionospheric parameters in the time period from January 2019 until December 2019. This period is part of the descending phase of the 24th solar cycle, which is defined by low solar and geomagnetic activity (Pesnell, 2016; Solomon et al., 2010). Two 27-day solar rotation periods from April 27, 2019 to May 24, 2019 and from May 23, 2019 to June 19, 2019 are analyzed in more detail.

2.1. Solar Radio Flux Index F10.7

The solar radio flux at a wavelength of 10.7 cm (F10.7) is a well-established solar activity index, which is used in several studies and ionospheric modeling approaches to indicate the solar activity level in general or as a proxy for the solar radiation at wavelengths that are difficult to measure (Tapping, 2013). F10.7 measures the total emission of the solar disk over a period of 1 h centered on the selected epoch (17:00, 20:00, 23:00 UT) and represents the full solar spectrum (Tapping, 2013; Tapping & Charrois, 1994). The ionospheric response to solar activity changes and its delay has been investigated in several studies based on F10.7 (Afraimovich et al., 2008; Jakowski et al, 1991, 2002; Lee et al., 2012; Min et al., 2009; Oinats et al., 2008;Titheridge, 1973; Zhang & Holt, 2008). F10.7 data are obtained from the NASA/GSFC's OMNI data set through the OMNIWeb interface (NASA, 2020).

2.2. Solar and Heliospheric Observatory

The Solar and Heliospheric Observatory (SOHO) Solar EUV Monitor (SEM) measures the solar EUV radiation continuously in two bands from 26 to 34 nm and from 0.1 to 50 nm (Judge et al., 1998; Zanna et al., 2015). This study uses the first order band which contains one of the strongest solar EUV emission lines (He II at 30.4 nm) and which impacts significantly the ionospheric state (Zanna et al., 2015). SEM data are obtained from the University of Southern California (USC) Space Sciences Center (NASA, 2020).

2.3. Global-Scale Observations of the Limb and Disk

GOLD measures different features of Earth's thermosphere and ionosphere allowing comprehensive studies of Earth's space environment and the upper atmosphere (Eastes et al., 2020). GOLD is an instrument retrieving measurements based on different scans of the sunlit disk, night disk, and limb (Eastes et al., 2017, 2020). The dayside disk measurements are used to derive neutral temperature, O/N_2 column density ratio and solar EUV flux proxy. The peak electron density is derived from the nightside disk measurements and the O_2 density profile is derived from stellar occultation measurements (NASA, 2020). The solar EUV flux proxy, the O/N_2 column density ratio and the peak electron density are of interest for this study on the ionospheric response to solar activity changes.

The satellite is in a geostationary orbit at 47.5°W and measures the full spectrum from 134 to 162 nm (Eastes et al., 2017) producing disk images from ±70° in latitude and longitude (at nadir) as well as limb measurements up to 600 km tangent altitude with different measurements modes (Eastes et al., 2017, 2020). The full disk images describing temperature and composition of the thermosphere at approximately 160 km are retrieved by combining scans of the north and south latitudes. Each scan of the full disk (30 min) ends

with a limb scan or an occultation if a bright star transits the limb (Eastes et al., 2020). The disk images of the thermospheric temperature at 60 min cadence have a precision of ±55 K and the disk images of the O/N_2 column density ratio at 30 min cadence have a precision of 10%. Both disk images are measured at 250 × 250 km^2 spatial resolution (Eastes et al., 2020). The peak electron density measurements of the equatorial arcs have a latitude resolution of 2° and precision of 10% (Eastes et al., 2020). The O_2 column density measurements at vertical resolution of 10 km have a precision of 10% above 150 km from stellar occultations (Eastes et al., 2020).

The solar EUV flux proxy Q_{EUV} describes the integrated solar irradiance below 45 nm and is derived from the far ultraviolet (FUV) measurements using a look-up-table. The O *I* 135.6 nm brightness, solar zenith angle and O/N_2 column density ratio are applied in this approach (NASA, 2020) according to algorithms by Strickland et al. (1995), Evans et al. (1995) and Strickland (2004). The sampling rate of Q_{EUV} is approximately 5 s (NASA, 2020).

The O/N_2 column density ratio of the thermospheric species O and N_2 is derived from the dayside measurements. The applied algorithms for this process were developed for data processing with Global Ultraviolet Imager (GUVI) and Special Sensor Ultraviolet Spectrographic Imager, but take advantage of the full spectrum measured by GOLD to reduce the signal-to-noise ratio (NASA, 2020). The approach is implemented according to algorithms by Strickland et al. (1995), Christensen (2003) and Strickland (2004).

GOLD performs scans of the nightside disk each day from 17:00 LT to 21:00 LT (corresponding to 47.5°W) and the peak electron density N_{Max} is directly derived from the O *I* 135.6 nm night glow emission measurements (NASA, 2020). This algorithm is based on the following assumptions: the ion-ion mutual neutralization is neglected, multiple scattering is neglected, the electron and O^+ densities are identical and the electron density profile is a Chapman layer profile (NASA, 2020).

The GOLD level 2 data products (solar EUV flux proxy Q_{EUV}, O/N_2 column density ratio and peak electron density N_{Max}) are provided by NASA through the GOLD Science Data Center (NASA, 2020).

2.4. Total Electron Content Maps

The International Global Navigation Satellite System (GNSS) Service (IGS) provides total electron content (TEC) maps of their associate analysis centers (Hernández-Pajares et al., 2009). The maps provide the vertical TEC, which is an integral measurement of the electron density covering the whole ionosphere and plasmasphere. This ionospheric parameter was used by several studies of the delayed ionospheric response to solar activity changes due to the 27-day solar rotation period (Afraimovich et al., 2008; Jacobi et al., 2016; Min et al., 2009; Oinats et al., 2008; Schmölter et al., 2018, 2020). Cai et al. (2020a, 2020) and showed a good correlation between TEC maps and N_{Max} maps. Thus, an investigation of the ionospheric response to solar activity changes based on comparison of IGS TEC maps and GOLD data is justified.

The present study uses the rapid high-rate solution (UHR) IGS TEC maps provided by the Universitat Politècnica de Catalunya (UPC). The sampling rate of these maps is 1 h and they are processed by applying a global voxel-defined 2-layer tomographic model solved with Kalman filter and spline interpolation (Hernndez-Pajares et al., 2016; Orús et al., 2005). The UHR TEC maps are provided by NASA through the Crustal Dynamics Data Information System (NASA, 2020).

3. Results

3.1. Comparison of Solar EUV Proxies and Measurements

The time series of F10.7, GOLD Q_{EUV} and SEM solar EUV flux in Figure 1 show differences between all three data sets from January 2019 to December 2019. There is an ongoing decrease of Q_{EUV} and solar EUV flux from April 2019 to July 2019 (approximately 10%) which is superimposed with stronger variations over shorter time periods. From July 2019 onward both data sets have an upward trend but Q_{EUV} increases stronger than the solar EUV flux. The described trend does not occur in the F10.7 data which instead show a constant trend superimposed with stronger variations over shorter time periods. A more detailed representation of the correlation between solar EUV flux and both proxies is shown in Figure 2 for different

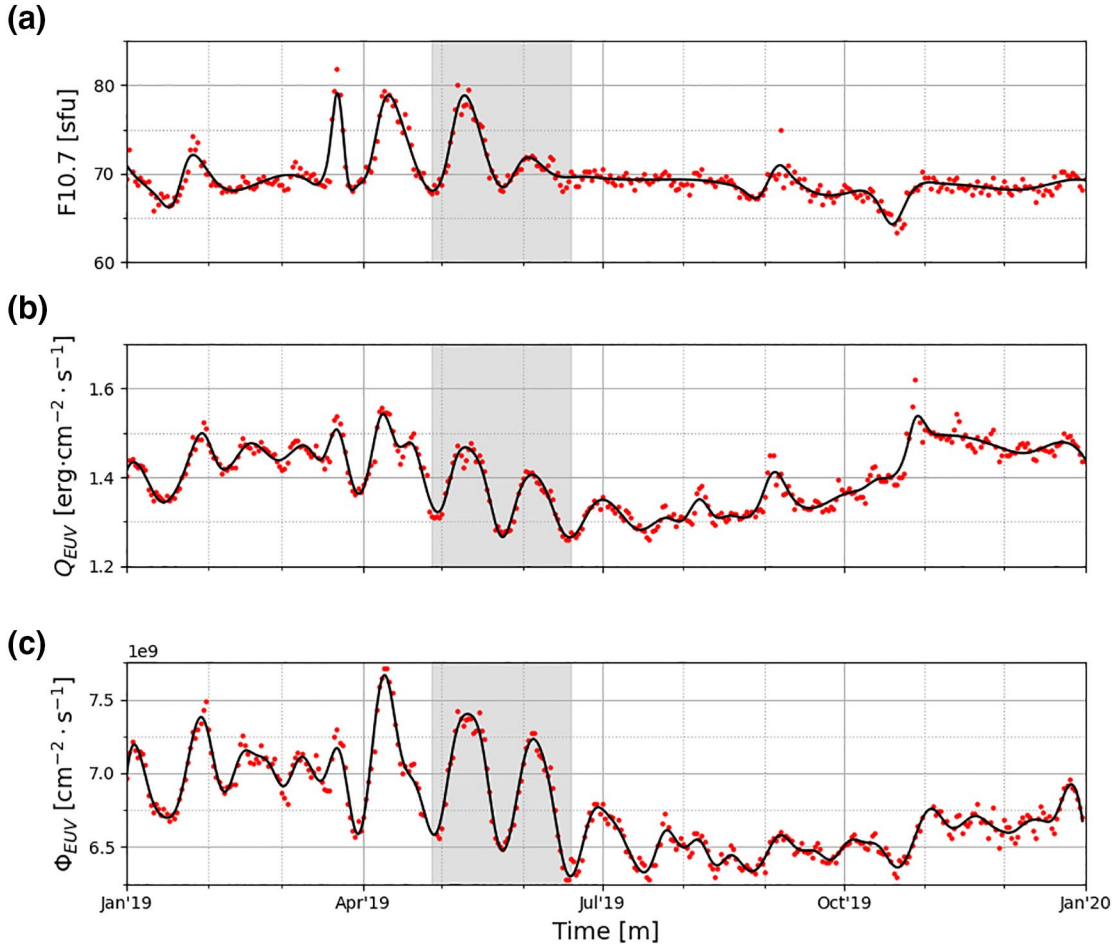

Figure 1. F10.7 (a), Q_{EUV} (b) and SEM solar EUV flux (c) are shown with red dots from January 2019 to December 2019. A smoothing spline interpolation is given in the plots (black line). The gray area marks the two 27-day solar rotation periods, which are analyzed in more detail. SEM, Solar EUV Monitor; EUV, extreme ultraviolet.

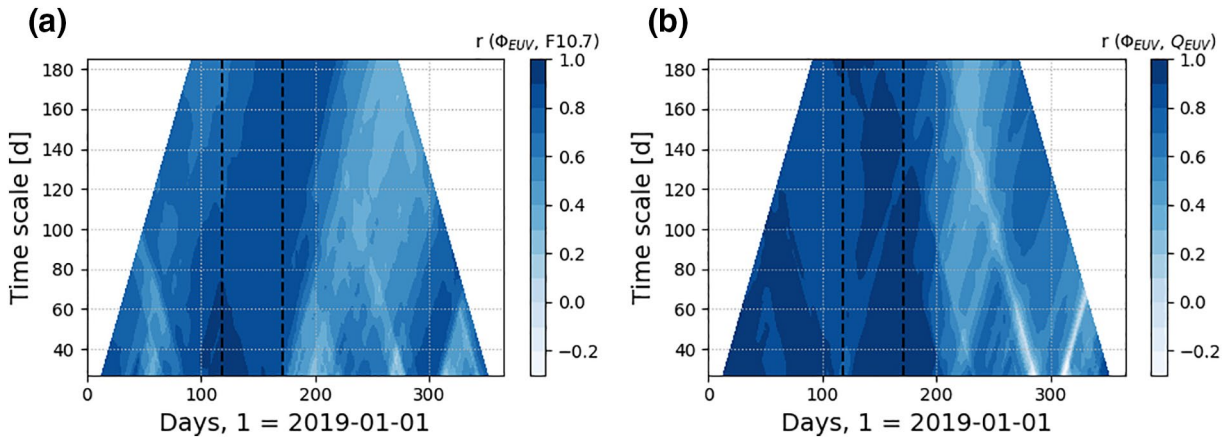

Figure 2. The correlation coefficients of solar EUV flux with F10.7 (a) and with Q_{EUV} (b) are shown for each day of the year 2019 at time scales from 27 to 185 days. The dashed lines mark the two 27-day solar rotation periods, which are analyzed in more detail. EUV, extreme ultraviolet.

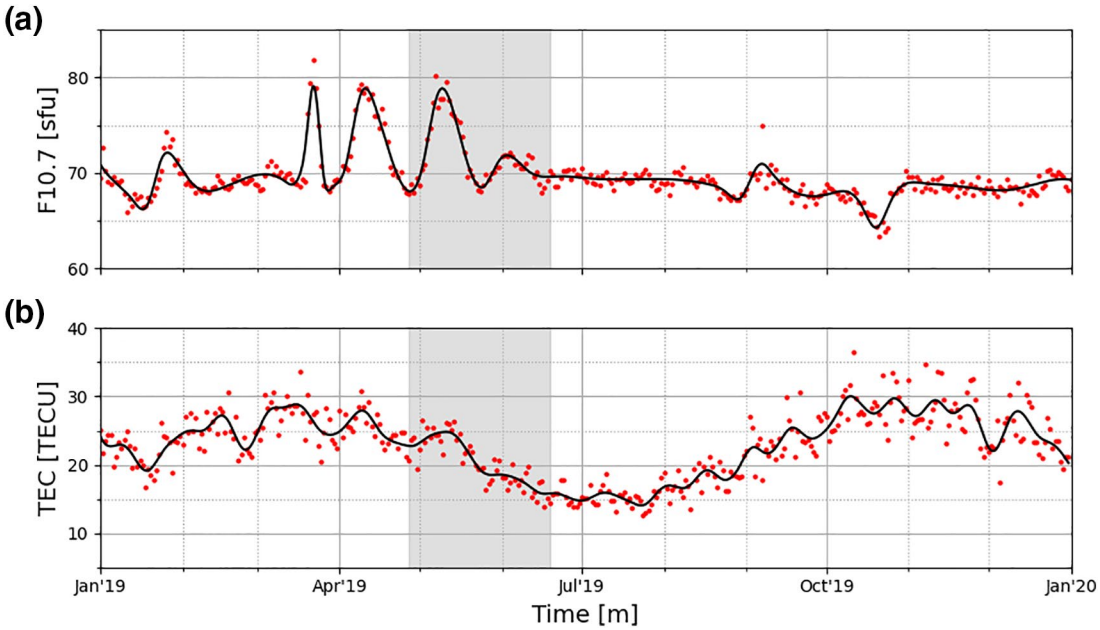

Figure 3. Comparison of daily F10.7 (a) and maximum TEC from 12:00 LT to 14:00 LT (b) is shown with red dots from January 2019 to December 2019. A smoothing spline interpolation is given in both plots (black line). The gray area marks the two 27-day solar rotation periods, which are analyzed in more detail. TEC, total electron content.

time scales at each day of the year. The correlation between the solar EUV flux and both proxies is especially strong from April 27, 2019 to June 19, 2019 with correlations coefficients of 0.85 for F10.7 and 0.97 for Q_{EUV}. This good correlation is due to two well-defined 27-day solar rotation periods occurring in each data set (see Figure 1). The first and second cycle vary approximately similar for the solar EUV flux and Q_{EUV} but are influenced by the ongoing decrease from April 2019 to July 2019. The difference between the first and second cycle is much stronger for F10.7 and a different trend is observed. This explains the lower correlation with the solar EUV flux. Nevertheless, all three time series represent the variations due to the 27-day solar rotation during this period and can be applied for an analysis of the delayed ionospheric response.

At longer time scales the correlation coefficients of F10.7 in Figure 2a decrease less than the correlation coefficients of Q_{EUV} in Figure 2b. This trend continues until F10.7 correlates even better with the solar EUV flux than Q_{EUV}. For example, for the whole year the correlation coefficient of solar EUV flux and F10.7 is 0.70 and the correlation coefficient of solar EUV flux and Q_{EUV} is 0.63.

3.2. Comparison of Solar Proxies and TEC

The correlation of solar proxies and TEC is known to vary with several parameters. Local time, geographic or geomagnetic coordinates, seasons and the solar cycle can have different impacts on the ionospheric response (TEC) to solar activity (F10.7, EUV) in each hemisphere (Bergeot et al., 2010; Liu & Chen, 2009). In order to investigate the ionospheric response to the solar activity changes within the 27-day solar rotation period a fixed location (geographic longitude of 0° and latitude of 0°) has been chosen. This allows the comparison of two well-defined 27-day solar rotation periods, which can be observed for maximum TEC from 12:00 LT to 14:00 LT.

Figure 3 shows the time series of F10.7 and maximum TEC from January 2019 to December 2019 as well as a smoothed spline interpolation of each data set. The interpolation is calculated using basis splines with chosen smoothing factors allowing the extraction of the 27-day solar rotation period. The seasonal variations of TEC in Figure 3b are much stronger than the variations due to the solar activity changes, but during two periods (from April 27, 2019 to May 24, 2019 and from May 23, 2019 to June 19, 2019) a noticeable correlation of F10.7 and TEC can be observed. In each time period a 27-day peak occurs in both data sets. During the first period F10.7 increases from approximately 70 to 80 sfu. The second period shows a smaller

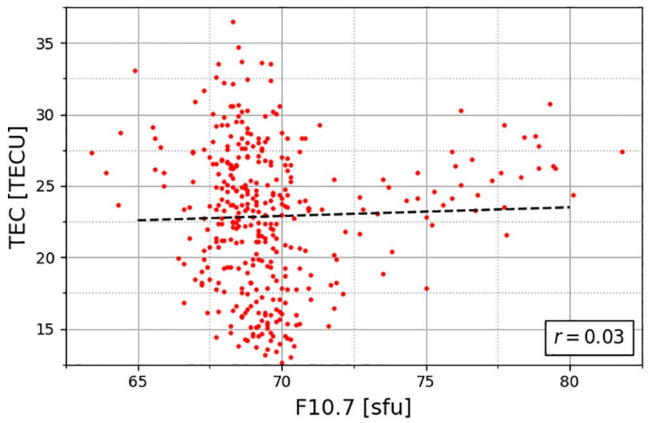

Figure 4. Scatter plot of daily F10.7 and corresponding TEC from January 2019 to December 2019. TEC, total electron content.

increase. Such well-defined increases with corresponding ionospheric responses are not observed during other periods of the year 2019. The corresponding peaks of TEC are superimposed with a constant decrease from March 2019 until July 2019. Figure 4 confirms that there is no direct correlation of F10.7 and TEC for the whole time period (correlation coefficient of 0.03). The correlation could be improved, for example, by removing seasonal and spatial variations of the TEC values. This is not needed for the further analysis though, since its focus are the discussed 27-day solar rotation periods, which appear in both data sets.

Figure 5a shows the selected solar EUV flux proxy Q_{EUV} from January 2019 to December 2019. TEC values in Figure 5b are selected at corresponding times of the Q_{EUV} measurements. The same interpolation as in Figure 3 is applied to retrieve smoothed trends. The difference between F10.7 in Figure 3a and Q_{EUV} in Figure 5a are most significant during the middle of the year. F10.7 has a negligible decrease during this time, but Q_{EUV} has a noticeable decrease of approximately 10% (see also Figure 1). The two periods from April 27, 2019 to May 24, 2019 and from May 23, 2019 to June 19, 2019 also show two significant peaks for each data set in Figure 5. Unlike the trend of F10.7, the peaks of Q_{EUV} are superimposed with an ongoing decrease similar to the trend of TEC. The correlation of Q_{EUV} and TEC is shown in Figure 6 for the whole time period (correlation coefficient of 0.69).

The significant changes of the solar activity from April 27, 2019 to May 24, 2019 and from May 23, 2019 to June 19, 2019 cause corresponding ionospheric variations (see gray areas in Figures 3 and 5). Therefore, these periods are appropriate for the analysis of the delayed ionospheric response. An analysis over longer periods (e.g., the whole year) would require the consideration of seasonal and spatial variations of the ionospheric state (TEC), but such a broad investigation is not aim of this study.

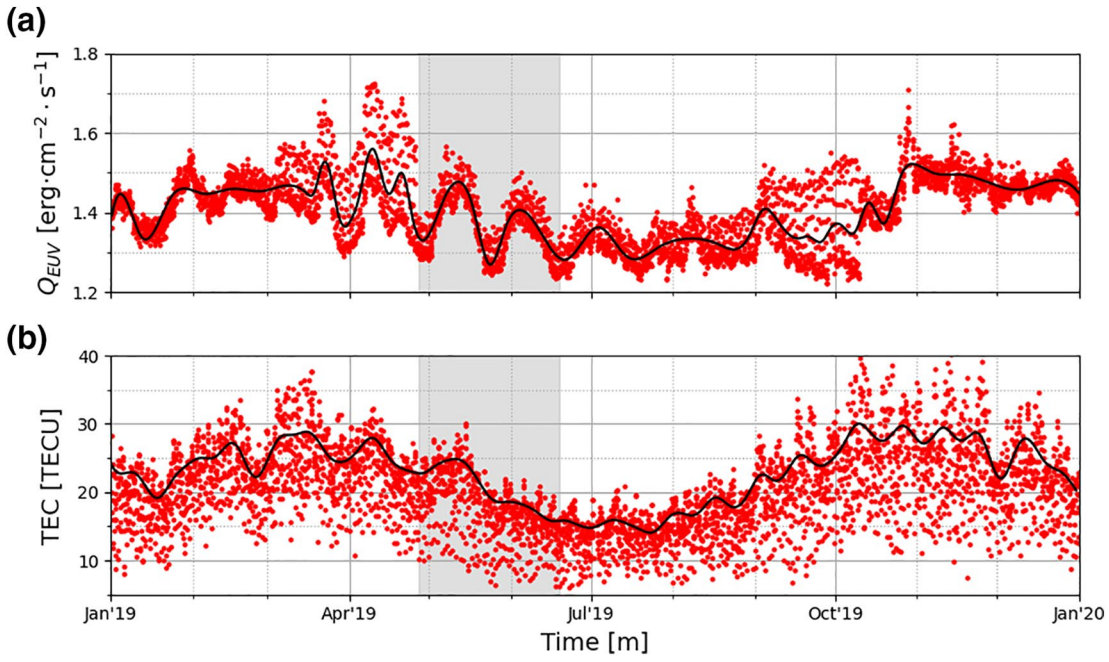

Figure 5. Comparison of Q_{EUV} (a) and corresponding TEC (b) is shown with red dots from January 2019 to December 2019. A smoothing spline interpolation is given in both plots (black line). The gray area marks the two 27-day solar rotation periods, which are analyzed in more detail. TEC, total electron content.

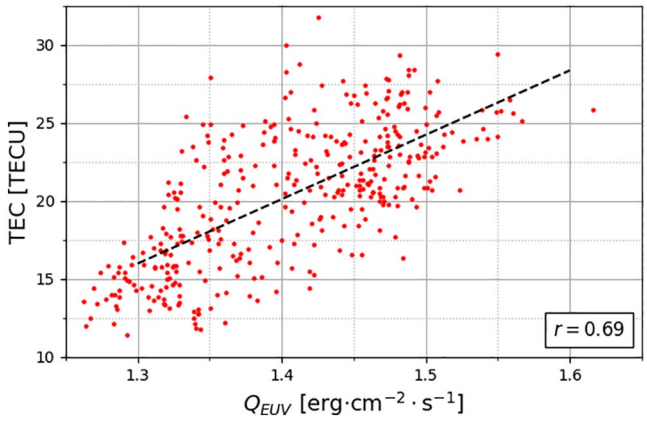

Figure 6. Scatter plot of daily Q_{EUV} and corresponding TEC from January 2019 to December 2019. TEC, total electron content.

3.3. Comparison of Peak Electron Density and TEC

Figure 7 shows the peak electron density N_{Max} and TEC in the available time period from March 2019 to December 2019. TEC values have been selected at measurement times of N_{Max} (from 17:00 LT to 21:00 LT). Therefore, a different situation compared to Figures 3 and 5 is presented, since at these times the ionosphere is dominated by recombination and not ionization (Rishbeth & Mendillo, 2001). This explains the lower TEC values in Figure 7 ($\overline{TEC}$ = 10.28 TECU) compared to Figure 3 ($\overline{TEC}$ = 22.86 TECU) and Figure 5 ($\overline{TEC}$ = 20.33 TECU). The correlation of N_{Max} and TEC is moderate (correlation coefficient of 0.59) and, thus, similar to the correlation of Q_{EUV} and TEC (see Figure 8). Spline interpolations are not applied to the data in Figure 7, since the deviations are stronger than the expected variations, for example, the 27-day solar rotation period.

3.4. Ionospheric Response to the 27-Day Solar Rotation Period

Figure 9 shows the correlations of the two chosen 27-day solar rotation periods, which are extracted from Figures 3 and 5. The correlation of F10.7 and corresponding TEC (correlation coefficient of 0.59) as well as Q_{EUV} and corresponding TEC (correlation coefficient of 0.55) are moderate. Especially, the correlation of F10.7 and corresponding TEC is improved for this shorter time period compared to the correlation for the year 2019 (see Figure 4). An additional trend is calculated for each data set, which removes the linear change of each time series during these periods. The resulting trends in Figure 10 (blue lines) are an acceptable approximation of the 27-day solar rotation period.

Each period is defined by a peak with corresponding peak time and maximum value which vary for each data set. The maximum values of F10.7 in Figures 10a and 10b, Q_{EUV} in Figures 10c and 10d as well as TEC in Figures 10e and 10f have differences of 6.92 sfu (≈8%), 0.07 erg cm^{-2} s^{-1} (≈4%) and 6.90 TECU (≈28%),

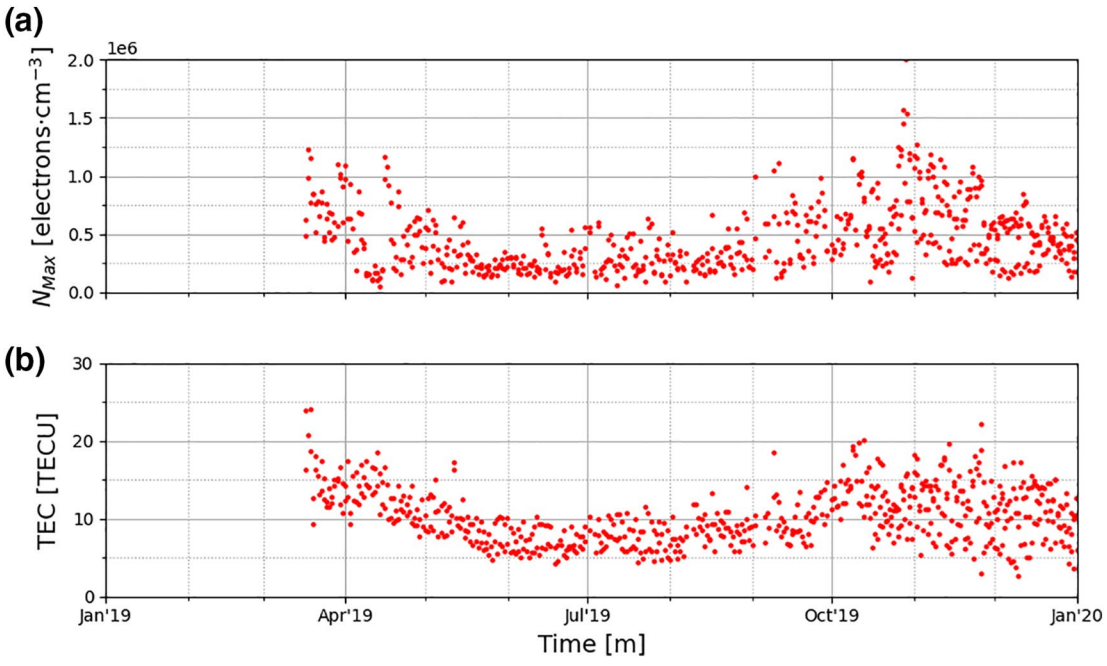

Figure 7. Comparison of N_{Max} (a) and corresponding TEC from 17:00 LT to 21:00 LT (b) is shown with red dots from March 2019 to December 2019. TEC, total electron content.

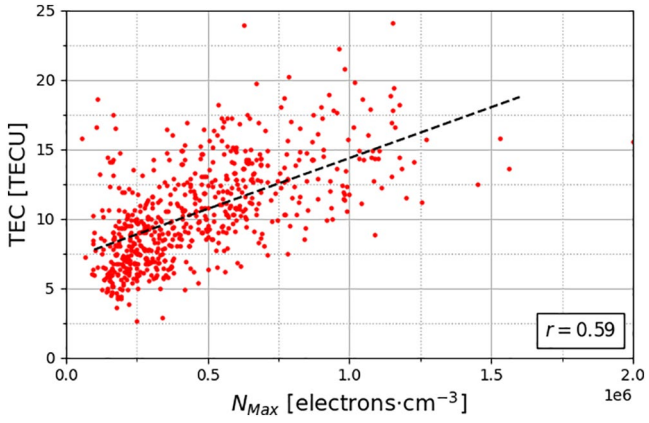

Figure 8. Scatter plot of daily N_{Max} and corresponding TEC from January 2019 to December 2019. TEC, total electron content.

respectively. These differences d for each parameter P are calculated according to

$$d(P) = \frac{\max(P_1) - \max(P_2)}{\max(P_1)} \tag{1}$$

and the differences between F10.7, Q_{EUV} and TEC can be ranked according to

$$d(Q_{\mathrm{EUV}}) < d(\mathrm{F10.7}) < d(\mathrm{TEC}) \tag{2}$$

The relative change of the ionosphere (TEC) is much stronger than the change in the solar activity (F10.7 and Q_{EUV}). The minimum values of F10.7 as well as Q_{EUV} do not show any significant difference between both periods. The TEC values in the second period are smaller than in the first period. This is due to the constant decrease of TEC from March 2019 until July 2019 seen in Figures 3b and 5b.

The peak time t_{max} of each Parameter P can be calculated by simply extracting the time of the maximum according to

$$t_{\mathrm{max}}(P) = \mathrm{argmax}(P). \tag{3}$$

The calculated peak times can be seen in Figure 10. The different peak times for both 27-day solar rotation periods can be related similar to Equation 2 by

$$t_{\mathrm{max}}(\mathrm{F10.7}) < t_{\mathrm{max}}(Q_{\mathrm{EUV}}) < t_{\mathrm{max}}(\mathrm{TEC}) \tag{4}$$

defining a delayed ionospheric response to the 27-day solar rotation period, which was investigated in preceding studies with similar observations or modeling results, for example, Ren et al. (2018). The delay τ can be specified using the solar activity proxy S (F10.7 or Q_{EUV}) and TEC according to

$$\tau(\mathrm{TEC}, S) = t_{\mathrm{max}}(\mathrm{TEC}) - t_{\mathrm{max}}(S). \tag{5}$$

The delay between TEC and F10.7 in Figures 10a and 10e is 3.13 days and the delay between TEC and F10.7 in Figures 10b and 10f is 2.42 days. These delays are much longer than calculated times in recent studies

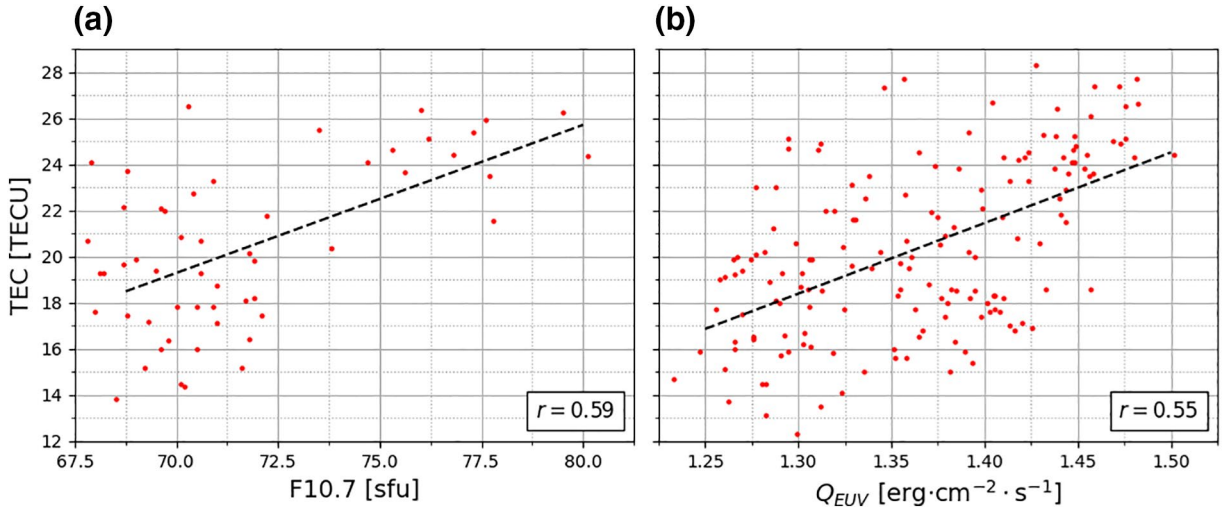

Figure 9. Scatter plots of daily F10.7 and corresponding TEC (a) as well as Q_{EUV} and corresponding TEC (b) from April 27, 2019 to June 19, 2019. TEC, total electron content.

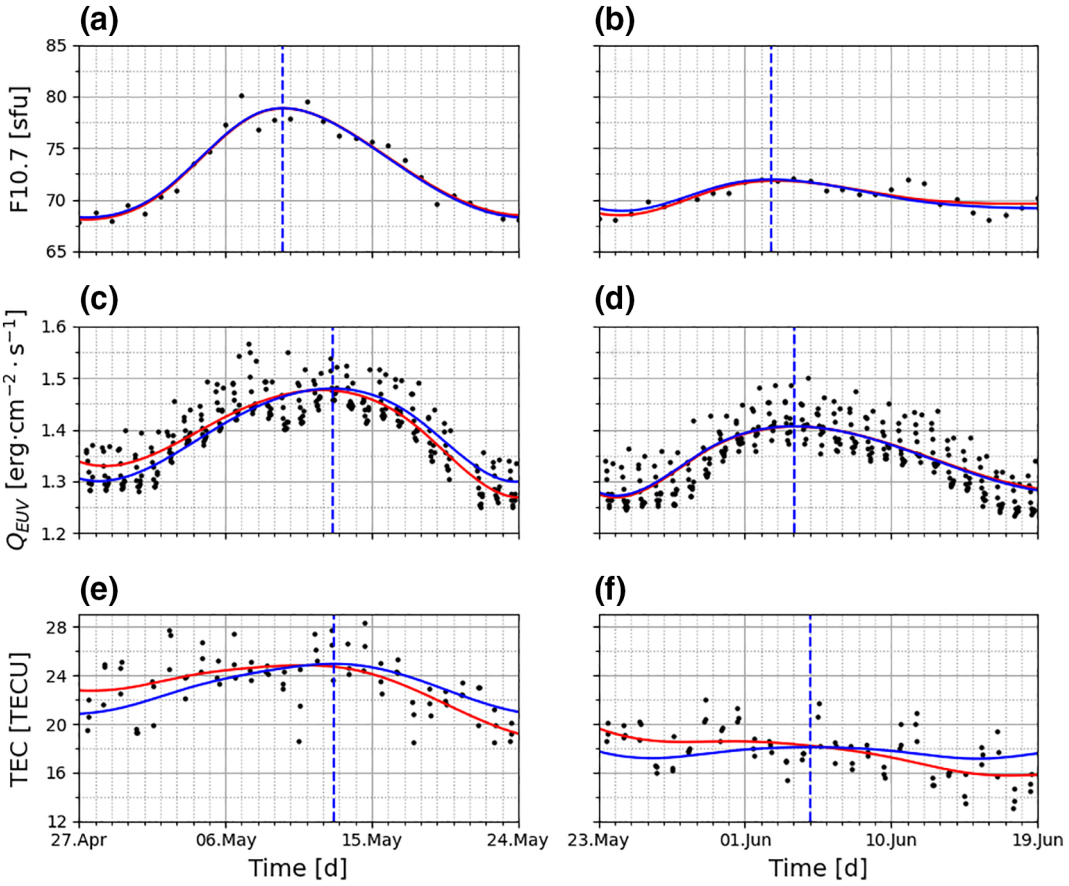

Figure 10. F10.7 (a), (b), Q_{EUV} (c), (d) and TEC (e), (f) are shown with black dots from April 27, 2019 to May 24, 2019 and from May 23, 2019 to June 19, 2019. The red line shows each basis spline interpolation that were calculated in Figures 3 and 5. The blue line shows each basis spline interpolation with the linear trend of each data set removed. The dashed blue lines mark the peak of these trends. TEC, total electron content.

(Ren et al., 2018; Schmölter et al., 2018, 2020), but similar values have been reported in older publications (Afraimovich et al., 2008; Jakowski et al., 2002; Lee et al., 2012; Min et al., 2009; Oinats et al., 2008; Zhang & Holt, 2008). The calculation process of the delay introduces uncertainties due to the applied basis spline interpolation and smoothing or due to the temporal resolution of the data. These uncertainties have a stronger impact for calculations using F10.7 which is measured at daily resolution. Nevertheless, the results can be used to compare the delayed ionospheric response during both 27-day solar rotation periods.

The delay between TEC and Q_{EUV} in Figures 10c and 10e is 0.08 days and the delay between TEC and Q_{EUV} in Figures 10d and 10f is 1.00 days. These results are much closer to calculated delays in recent studies (Ren et al., 2018; Schmölter et al., 2018, 2020). The mentioned influence of uncertainties caused by the interpolation process is less due to the higher sampling rate of Q_{EUV} compared to F10.7. Therefore, a smaller difference to studies based on EUV measurements is expected, for example, Schmölter et al. (2020).

The delayed ionospheric response to the 27-day solar rotation period can also be estimated with cross-correlation analysis (Schmölter et al., 2018, 2020). This method fits the data for the whole time period and the calculated results are expected to be different to the delay estimated based on the peak time of the 27-day solar rotation period. The cross-correlation analysis does not require any filtering of the data and therefore no basis spline interpolation is applied. The cross-correlation for a solar proxy S and the ionospheric state P given by maximum TEC is calculated by

$$\left(P * S\right)_{k-N+1} = \sum_{i=0}^{N-1} P_i \cdot S^*_{i=k+N-1} \tag{6}$$

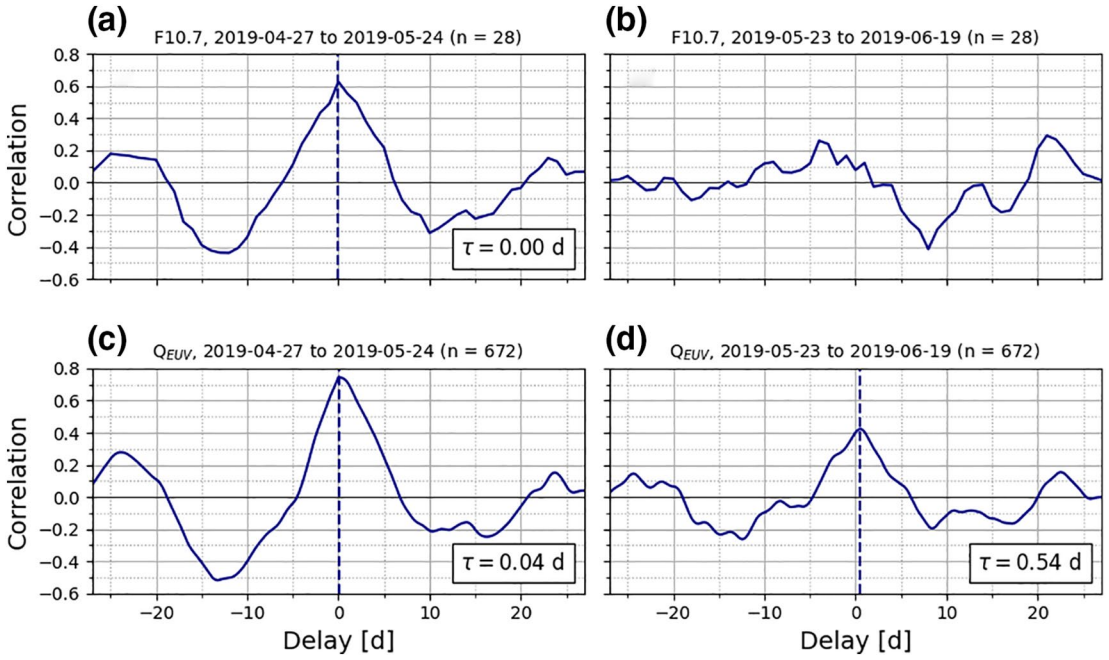

Figure 11. Cross-correlations of TEC with F10.7 (a), (b) and Q_{EUV} (c), (d) are shown from April 27, 2019 to May 24, 2019 and from May 23, 2019 to June 19, 2019. The dashed lines mark the maximum correlation and the lag. The sampling rates are 1 day (a), (b) and 1 h (c), (d). TEC, total electron content.

and the delay is estimated according to

$$\tau(P,S) = \text{argmax}\left((\text{P} * \text{S})\right) \tag{7}$$

The sampling rate of the estimated cross-correlation is defined by the input data set with the lower sampling rate. Therefore, the results based on F1.07 and TEC have a sampling rate of 1 day and the results based on Q_{EUV} and TEC have a sampling rate of 1 h. The delay estimation by cross-correlation analysis benefits from the higher resolution of Q_{EUV}.

The results of the cross-correlation analysis for both solar proxies from April 27, 2019 to May 24, 2019 and from May 23, 2019 to June 19, 2019 are shown in Figure 11. The most significant difference compared to the results in Figure 10 is the cross-correlation based on F10.7 for the second period in Figure 11b. The cross-correlation has no pronounced peak and a reasonable estimation of a delay is not possible in this case. The first period in Figure 11a shows a delay of 0 days. The differences of the results compared to the trends in Figure 10 are most likely due to the lack of smoothing leading to the inclusion of smaller features in this approach. The results of the cross-correlation analysis based on Q_{EUV} have a pronounced peak for both periods and delays of 1 and 13 h are estimated. These delays are also different from the trends in Figure 10 but the increase of the delay during the second period is confirmed. As explained, the comparison of peak times and the cross-correlation analysis describe different delays, but the benefit of higher sampling rates is greater with the cross-correlation analysis.

The results in Figures 10 and 11 confirm previous studies. The solar activity is a driving factor of the delayed ionospheric response (Ren et al., 2018; Schmölter et al., 2020) which is impacted by its change even during a solar minimum with low solar and geomagnetic activity. The O/N_2 column density ratio also influences the response time of the ionosphere to solar activity changes (Ren et al., 2018) and is even more important during the chosen time periods with low solar activity (Rishbeth, 1998). Figure 12 shows the O/N_2 column density ratio from April 27, 2019 to May 24, 2019 and from May 23, 2019 to June 19, 2019. The O/N_2 column density ratio trend does not correlate with the two observed 27-day solar rotation periods (correlation coefficient of 0.24 with F10.7 and correlation coefficient of 0.06 with Q_{EUV}). The occurring variations are on smaller time scales and and no general trend for the whole periods can be reliably estimated. Therefore, only the mean values of each time period are compared. The mean O/N_2 column density ratio decreases

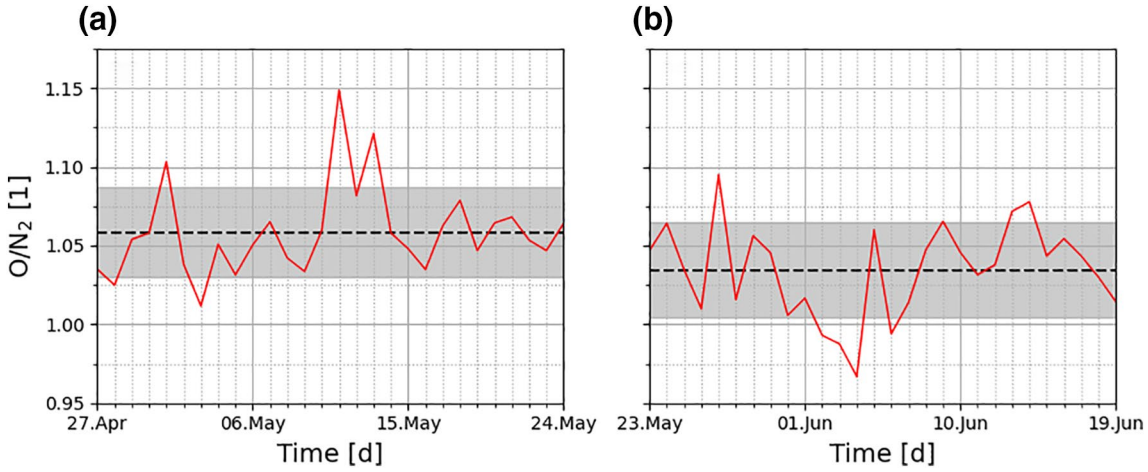

Figure 12. The O/N_2 column density ratio from 12:00 LT to 14:00 LT is shown with red lines from April 27, 2019 to May 24, 2019 and from May 23, 2019 to June 19, 2019. The black dashed line marks the mean value of each period and the gray area indicates standard deviation.

from 1.06 in the first period to 1.03 in the second period (approximately 3%). This trend could be related to the to the ongoing decrease of the solar activity from March 2019 to July 2019 that is superimposed with the analyzed 27-day solar rotation periods (see Figures 1b and 1c), but other processes could impact the O/N_2 column density ratio as well, for example, temperature, density, or wind changes caused by atmospheric waves (He et al., 2010).

The O/N_2 column density ratio is known to modulate the ionospheric response time (Ren et al., 2018) and to be impacted by the change of solar activity itself (Luan et al., 2017). The influence of solar activity and O/N_2 column density ratio is defined according to Equation 8 which describes the photochemical equilibrium in the F region (Rishbeth, 1998).

$$n \sim \frac{q}{\beta} \sim \frac{I_\infty [\mathrm{O}]}{k'[\mathrm{O_2}] + k''[\mathrm{N_2}]} \tag{8}$$

The electron density n is given by ion production q and loss β. The production is defined by the atomic oxygen concentration [O] and the factor I_∞ that is proportional to the flux of solar ionizing radiation (Rishbeth, 1998). The loss is defined by the molecular oxygen concentration $[O_2]$ and the molecular nitrogen concentration $[N_2]$ with two corresponding coefficients k (Rishbeth, 1998). The solar activity controls directly the production and the O/N_2 column density ratio controls production as well as loss. An increase of the production caused by a solar activity increase, an O/N_2 column density ratio increase or both relates to a longer ionospheric response time (Ren et al., 2018; Schmölter et al., 2020).

The solar activity and its change is stronger during the period from April 27, 2019 to May 24, 2019 compared to the period from May 23, 2019 to June 19, 2019. A longer response time for the first period is expected according to this difference and the established understanding (considering only the response to the 27-day solar rotation period). The O/N_2 column density ratio is also increased during the first period but the difference is not significant enough to analyze the influence on the delayed ionospheric response. In addition, the processes controlling the O/N_2 column density ratio are complex (He et al., 2010; Luan et al., 2017) and the characterization of their impact would require an extensive analysis that is beyond the scope of this study, for example, a spatial analysis for different regions covered by GOLD measurements.

τ(TEC, F10.7) decreases 0.71 days for the second time period in Figure 10, but the cross-correlation analysis in Figure 6 cannot confirm this. τ(TEC, Q_{EUV}) increases 0.92 days in Figure 10 and 0.50 days in Figure 11 for the second time period. Considering the good correlation of Q_{EUV} in the chosen time period with actual solar EUV flux measurements (see Figures 1 and 2) and the moderate correlation with TEC (see Figure 9) the delays estimated based on this parameter are expected to be more reliable. Therefore, the change of the delay does not align with expectations which could be due to various processes impacting the ionospheric

state (e.g., plasma transport due to the equatorial plasma fountain effect) or due to uncertainties in the applied methods. The more complex changes of the O/N_2 column density ratio in Figure 12 could also explain parts of the observed trend, but the estimated delays are not precise enough to perform such an analysis (e.g., due to the sampling rate). The overall O/N_2 column density ratio trend follows the TEC variations though, which is of interest for future studies to analyze the seasonal variations of the delayed ionospheric response in more detail (Schmölter et al., 2020). Especially, the combination of different GOLD data (solar EUV flux proxy Q_{EUV}, O/N_2 column density ratio and eventually O_2 density profile) allows a comprehensive analysis when longer time periods of data are available, for example, by applying superposed epoch analysis.

4. Conclusion

The analysis of F10.7, Q_{EUV}, N_{Max}, O/N_2 column density and TEC has given a first impression of the capabilities of GOLD data in analyzing the delayed ionospheric response to the 27-day solar rotation period. The following results were obtained in the current study and represent an important starting point for future research in this area:

1. The solar proxies F10.7 and Q_{EUV} show noticeable differences, but are in good agreement for at least two solar rotation periods during the year 2019. The delayed ionospheric response time to the 27-day solar rotation periods from April 27, 2019 to May 24, 2019 and from May 23, 2019 to June 19, 2019 could be retrieved using both data sets (see Figure 10). Q_{EUV} is a more reliable proxy than F10.7, which is not synchronized with the solar EUV radiation at all times (Chen et al., 2011, 2018). Therefore, Q_{EUV} should be used in data analyses of the ionospheric response to solar activity changes but also for ionospheric modeling approaches
2. Q_{EUV} and corresponding TEC are in good agreement (correlation coefficient of 0.69). The estimated delays based on Q_{EUV} and TEC are similar to the results of studies using actual EUV measurements and TEC, for example, Schmölter et al. (2020)
3. N_{Max} and corresponding TEC are in good agreement (correlation coefficient of 0.59). The daily GOLD measurements of N_{Max} from 17:00 LT to 21:00 LT are of interest to analyze accumulation processes within the delayed ionospheric response
4. The O/N_2 column density ratio provides additional information to the analysis of the delayed ionospheric response considering its importance as shown in preceding studies (Ren et al., 2018; Schmölter et al., 2020). An analysis of longer periods with varying solar activity and O/N_2 column density ratio conditions might allow to estimate their respective impact on the delay
5. It is important to investigate the different ionospheric processes during ionization and recombination periods of the 27-day solar rotation period based on maximum and late noon TEC. GOLD data (Q_{EUV}, N_{Max} and O/N_2 column density ratio) provide critical additional information exactly during these periods
6. Delays τ(TEC, F10.7) of 3.13 and 2.42 days and delays τ(TEC, Q_{EUV}) of 0.08 and 1.00 days are estimated by comparison of the peak times of the two 27-day solar rotation periods from April 27, 2019 to May 24, 2019 and from May 23, 2019 to June 19, 2019. The results based on Q_{EUV} are qualitatively confirmed with a cross-correlation analysis that estimates respective delays of 0.04 and 0.54 days

GOLD data offer the potential to gain more knowledge about the response of the ionosphere to solar activity and to better characterize the occurring delay. The combination of different parameters can contribute to identify their respective impacts on the ionospheric delay. In conclusion, we strongly recommend to include GOLD data in future studies of the delayed ionospheric response to solar EUV radiation.

Data Availability Statement

F10.7 data are provided by NASA through https://omniweb.gsfc.nasa.gov/form/dx1.html, SOHO SEM data are provided by the USC Space Sciences Center through https://dornsifecms.usc.edu/space-sciences-center/download-sem-data/, GOLD data are provided by NASA through https://gold.cs.ucf.edu/data/search/, UHR TEC maps are provided by NASA through https://cddis.nasa.gov/archive/gnss/products/ionex/.

Acknowledgments
The authors thank NASA for making F10.7, SOHO SEM and GOLD data as well as UHR TEC maps publicly available.

References

Afraimovich, E. L., Astafyeva, E. I., Oinats, A. V., Yasukevich, Y. V., & Zhivetiev, I. V. (2008). Global electron content: A new conception to track solar activity. *Annales Geophysicae*, *26*(2), 335–344. https://doi.org/10.5194/angeo-26-335-2008

Bergeot, N., Legrand, J., Burston, R., Bruyninx, C., Defraigne, P., Chevalier, J.-M., et al. (2010). Correlation between solar activity and Earth's ionospheric electron content during the 23rd solar cycle. *AGU Fall Meeting Abstracts*, *2010*, SA33B-1774

Cai, X., Burns, A., Wang, W., Coster, A., Qian, L., Liu, J., et al. (2020). Comparison of GOLD nighttime measurements of OI 135.6 nm radiance with the total electron content map: Preliminary results. *AGU 2019 Fall Meeting*. https://doi.org/10.1002/essoar.10502268.1

Cai, X., Burns, A. G., Wang, W., Coster, A., Qian, L., Liu, J., et al. (2020). Comparison of GOLD nighttime measurements with total electron content: Preliminary results. *Journal of Geophysical Research: Space Physics*, *125*(9), e2019JA027767–e2019JA027767. https://doi.org/10.1029/2019ja027767

Chen, Y., Liu, L., Le, H., & Wan, W. (2018). Responses of solar irradiance and the ionosphere to an intense activity region. *Journal of Geophysical Research: Space Physics*. *123*(3), 2116–2126. https://doi.org/10.1002/2017ja024765

Chen, Y., Liu, L., & Wan, W. (2011). Does the F10.7index correctly describe solar EUV flux during the deep solar minimum of 2007-2009? *Journal of Geophysical Research*, *116*(A4). https://doi.org/10.1029/2010ja016301

Christensen, A. B. (2003). Initial observations with the Global Ultraviolet Imager (GUVI) in the NASA TIMED satellite mission. *Journal of Geophysical Research*, *108*(A12). https://doi.org/10.1029/2003ja009918

Eastes, R. W., McClintock, W. E., Burns, A. G., Anderson, D. N., Andersson, L., Aryal, S., et al. (2020). Initial observations by the GOLD mission. *Journal of Geophysical Research: Space Physics*, *125*(7), e2020JA027823–e2020JA027823. https://doi.org/10.1029/2020ja027823

Eastes, R. W., McClintock, W. E., Burns, A. G., Anderson, D. N., Andersson, L., Codrescu, M., et al. (2017). The Global-Scale Observations of the Limb and Disk (GOLD) mission. *Space Science Reviews*, *212*(1–2), 383–408. https://doi.org/10.1007/s11214-017-0392-2

Evans, J. S., Strickland, D. J., & Huffman, R. E. (1995). Satellite remote sensing of thermospheric O/N2and Solar EUV: 2. Data analysis. *Journal of Geophysical Research*, *100*(A7), 12227–12233. https://doi.org/10.1029/95ja00573

Forbes, J. M., Palo, S. E., & Zhang, X. (2000). Variability of the ionosphere. *Journal of Atmospheric and Solar-Terrestrial Physics*, *62*(8), 685–693. https://doi.org/10.1016/s1364-6826(00)00029-8

He, M., Liu, L., Wan, W., Lei, J., & Zhao, B. (2010). Longitudinal modulation of the O/N2column density retrieved from TIMED/GUVI measurement. *Geophysical Research Letters*, *37*(20). https://doi.org/10.1029/2010gl045105

Hernández-Pajares, M., Juan, J. M., Sanz, J., Orus, R., Garcia-Rigo, A., Feltens, J., et al. (2009). The IGS VTEC maps: A reliable source of ionospheric information since 1998. *Journal of Geodesy*, *83*(3–4), 263–275. https://doi.org/10.1007/s00190-008-0266-1

Hernndez-Pajares, M., Roma-Dollase, D., Krankowski, A., Ghoddousi-Fard, R., Yuan, Y., Li, Z., et al. (2016). Comparing performances of seven different global VTEC ionospheric models in the IGS context. *IGS workshop* 8–12. https://doi.org/10.13140/RG.2.1.2378.2168 February 2016

Jacobi, C., Jakowski, N., Schmidtke, G., & Woods, T. N. (2016). Delayed response of the global total electron content to solar EUV variations. *Advances in Radio Science*, *14*, 175–180. https://doi.org/10.5194/ars-14-175-2016

Jakowski, N., Fichtelmann, B., & Jungstand, A. (1991). Solar activity control of ionospheric and thermospheric processes. *Journal of Atmospheric and Terrestrial Physics*, *53*(11), 1125–1130. https://doi.org/10.1016/0021-9169(91)90061-B, The 7th International Scostep symposium on Solar-Terrestrial Physics.

Jakowski, N., Heise, S., Wehrenpfennig, A., Schlter, S., & Reimer, R. (2002). GPS/GLONASS-based TEC measurements as a contributor for space weather forecast. *Journal of Atmospheric and Solar-Terrestrial Physics*, *64*(5–6), 729–735. https://doi.org/10.1016/s1364-6826(02)00034-2

Judge, D. L., McMullin, D. R., Ogawa, H. S., Hovestadt, D., Klecker, B., Hilchenbach, M., et al. (1998). First solar EUV irradiances obtained from SOHO by the CELIAS/SEM. In: *Solar Electromagnetic Radiation Study for Solar Cycle*, Springer Netherlands, 22, 161–173. https://doi.org/10.1007/978-94-011-5000-2_12

Kane, R. P., de Paula, E. R., & Trivedi, N. B. (1995). Variations of solar EUV, UV and ionospheric foF2 related to the solar rotation period. *Annales Geophysicae*, *13*(7), 717–723. https://doi.org/10.1007/s00585-995-0717-4

Kelley, M. (2009). *The Earth's ionosphere*, San Diego: Academic Press, Vol. 96. https://doi.org/10.1016/B978-0-12-404013-7.X5001-1

Lee, C.-K., Han, S.-C., Bilitza, D., & Seo, K.-W. (2012). Global characteristics of the correlation and time lag between solar and ionospheric parameters in the 27-day period. *Journal of Atmospheric and Solar-Terrestrial Physics*, *77*, 219–224. https://doi.org/10.1016/j.jastp.2012.01.010

Liu, L., & Chen, Y. (2009). Statistical analysis of solar activity variations of total electron content derived at Jet Propulsion Laboratory from GPS observations. *Journal of Geophysical Research*, *114*(A10). https://doi.org/10.1029/2009ja014533

Luan, X., Wang, W., Burns, A., & Dou, X. (2017). Solar cycle variations of thermospheric O/N 2 longitudinal pattern from TIMED/GUVI. *Journal of Geophysical Research: Space Physics*, *122*(2), 2605–2618. https://doi.org/10.1002/2016ja023696

Ma, R., Xu, J., Wang, W., & Lei, J. (2012). The effect of ~27 day solar rotation on ionosphericF2region peak densities (NmF2). *Journal of Geophysical Research*, *117*(A3). https://doi.org/10.1029/2011ja017190

Min, K., Park, J., Kim, H., Kim, V., Kil, H., Lee, J., et al. (2009). The 27-day modulation of the low-latitude ionosphere during a solar maximum. *Journal of Geophysical Research*, *114*(A4), A04317. https://doi.org/10.1029/2008JA013881

NASA (2020). *GNSS atmospheric products*, Greenbelt: NASA CDDIS. Retrieved from https://cddis.nasa.gov/archive/gnss/products/ionex/ Last access 14.12.2020.

NASA (2020). *GOLD data download*, Greenbelt: NASA/Goddard Space Flight Center. Retrieved from https://gold.cs.ucf.edu/data/search/ Last access 11.09.2020.

NASA (2020). *GOLD science data products guide – rev 3.0*, Greenbelt: NASA/Goddard Space Flight Center. Retrieved from https://gold.cs.ucf.edu/wp-content/documentation/GOLD_Public_Science_Data_Products_Guide_Rev3.0.pdf Last access 14.08.2019.

NASA (2020). *OMNIWeb interface – F10.7*, Greenbelt: NASA/Goddard Space Flight Center. Retrieved from https://omniweb.gsfc.nasa.gov/form/dx1.html Last access 11.09.2020.

NASA (2020). *USC space Sciences center – data*, Los Angeles: USC Space Sciences Center. Retrieved from https://dornsifecms.usc.edu/space-sciences-center/download-sem-data/Last access 16.11.2020.

Oinats, A. V., Ratovsky, K. G., & Kotovich, G. V. (2008). Influence of the 27-day solar flux variations on the ionosphere parameters measured at Irkutsk in 20032005. *Advances in Space Research*, *42*(4), 639–644. https://doi.org/10.1016/j.asr.2008.02.009

Orús, R., Hernández-Pajares, M., Juan, J. M., & Sanz, J. (2005). Improvement of global ionospheric VTEC maps by using kriging interpolation technique. *Journal of Atmospheric and Solar-Terrestrial Physics*, *67*(16), 1598–1609. https://doi.org/10.1016/j.jastp.2005.07.017

Pesnell, W. D. (2016). Predictions of solar cycle 24: How are we doing? *Space Weather*, *14*(1), 10–21. https://doi.org/10.1002/2015sw001304

Ren, D., Lei, J., Wang, W., Burns, A., Luan, X., & Dou, X. (2018). Does the peak response of the ionospheric F 2 region plasma lag the peak of 27-day solar flux variation by multiple days? *Journal of Geophysical Research: Space Physics*, *123*(9), 7906–7916. https://doi.org/10.1029/2018JA025835

Ren, D., Lei, J., Wang, W., Burns, A., Luan, X., & Dou, X. (2019). A simulation study on the time delay of daytime thermospheric temperature response to the 27-day solar EUV flux variation. *Journal of Geophysical Research: Space Physics*, *124*(11), 9184–9193. https://doi.org/10.1029/2019ja027000

Ren, D., Lei, J., Wang, W., Burns, A., Luan, X., & Dou, X. (2020). Different peak response time of daytime thermospheric neutral species to the 27-day solar EUV flux variations. *Journal of Geophysical Research: Space Physics*, *125*(7), e2020JA027840–e2020JA027840. https://doi.org/10.1029/2020ja027840

Rich, F. J. (2003). The 27-day variations of plasma densities and temperatures in the topside ionosphere. *Journal of Geophysical Research*, *108*(A7). https://doi.org/10.1029/2002ja009731

Rishbeth, H. (1998). How the thermospheric circulation affects the ionospheric F2-layer. *Journal of Atmospheric and Solar-Terrestrial Physics*, *60*(14), 1385–1402. https://doi.org/10.1016/S1364-6826(98)00062-5

Rishbeth, H., & Mendillo, M. (2001). Patterns of F2-layer variability. *Journal of Atmospheric and Solar-Terrestrial Physics*, *63*(15), 1661–1680. https://doi.org/10.1016/S1364-6826(01)00036-0

Schmölter, E., Berdermann, J., Jakowski, N., & Jacobi, C. (2020). Spatial and seasonal effects on the delayed ionospheric response to solar EUV changes. *Annales Geophysicae*, *38*(1), 149–162. https://doi.org/10.5194/angeo-38-149-2020

Schmölter, E., Berdermann, J., Jakowski, N., Jacobi, C., & Vaishnav, R. (2018). Delayed response of the ionosphere to solar EUV variability. *Advances in Radio Science*, *16*, 149–155. https://doi.org/10.5194/ars-16-149-2018

Solomon, S. C., Woods, T. N., Didkovsky, L. V., Emmert, J. T., & Qian, L. (2010). Anomalously low solar extreme-ultraviolet irradiance and thermospheric density during solar minimum. *Geophysical Research Letters*, *37*(16). https://doi.org/10.1029/2010gl044468

Strickland, D. J. (2004). Solar EUV irradiance variability derived from terrestrial far ultraviolet dayglow observations. *Geophysical Research Letters*, *31*(3). https://doi.org/10.1029/2003gl018415

Strickland, D. J., Evans, J. S., & Paxton, L. J. (1995). Satellite remote sensing of thermospheric O/N2 and solar EUV: 1. Theory. *Journal of Geophysical Research*, *100*(A7), 12217–12226. https://doi.org/10.1029/95ja00574

Tapping, K. F. (2013). The 10.7 cm solar radio flux (F10.7). *Space Weather*, *11*(7), 394–406. https://doi.org/10.1002/swe.20064

Tapping, K. F., & Charrois, D. P. (1994). Limits to the accuracy of the 10.7 cm flux. *Solar Physics*, *150*(1–2), 305–315. https://doi.org/10.1007/bf00712892

Titheridge, J. E. (1973). The electron content of the southern mid-latitude ionosphere, 1965–1971. *Journal of Atmospheric and Terrestrial Physics*, *35*(5), 981–1001. https://doi.org/10.1016/0021-9169(73)90077-9

Vaishnav, R., Jacobi, C., & Berdermann, J. (2019). Long-term trends in the ionospheric response to solar extreme-ultraviolet variations. *Annales Geophysicae*, *37*(6), 1141–1159. https://doi.org/10.5194/angeo-37-1141-2019

Zanna, G. D., Wieman, S. R., Andretta, V., & Didkovsky, L. (2015). The EUV spectrum of the Sun: SOHO, SEM, and CDS irradiances. *Astronomy & Astrophysics*, *581*. A25. https://doi.org/10.1051/0004-6361/201526227

Zhang, S.-R., & Holt, J. M. (2008). Ionospheric variability from an incoherent scatter radar long-duration experiment at Millstone Hill. *Journal of Geophysical Research*, *113*(A3). https://doi.org/10.1029/2007ja012639